Including Antenna Models in Microwave Imaging for Breast-Cancer Screening

Rubæk, Tonny; Meincke, Peter

Published in:
Proceedings of the EuCAP - European Conference on Antennas and Propagation

Link to article, DOI:
10.1109/EUCAP.2006.4584912

Publication date:
2006

Document Version
Publisher's PDF, also known as Version of record

INCLUDING ANTENNA MODELS IN MICROWAVE IMAGING FOR BREAST CANCER SCREENING

Tonny Rubæk and Peter Meincke

Technical University of Denmark, Ørsteds Plads, Building 348, DK-2800 Kgs. Lyngby, Denmark,
Email: [tru/pme]@oersted.dtu.dk

ABSTRACT

Microwave imaging is emerging as a tool for screening for breast cancer, but the lack of methods for including the characteristics of the antennas of the imaging systems in the imaging algorithms limits their performance. In this paper, a method for incorporating the full antenna characteristics, in terms of the transmission-matrix representation, in a frequency-domain imaging algorithm is presented. The algorithm is tested on a simulation of the Physical-Anomaly Tomography (PAT) scanner imaging system developed at the Technical University of Denmark and is shown to have superior performance when compared to a simple algorithm in which the antennas are assumed to be ideal dipoles.

1. INTRODUCTION

During the last decade, the use of microwave imaging as a screening tool for detection of breast cancer has gained the attention of an increasing number of research groups [1–5]. The use of microwave imaging is seen as an appealing alternative or supplement to the widely used X-ray mammography for two main reasons. First, the microwaves are non-ionizing, and therefore less hazardous to the health of the women being screened. Second, the physical parameters creating contrast in the microwave region are different from those creating the contrast in X-ray images. This implies that tumors that are not visible in the X-ray images mmight be detectable when using microwave imaging, thus possibly allowing for the screening of the breasts of premenopausal women.

One of the difficulties encounteredwhen creating imaging algorihtms for microwave-imaging systems is the incorporation of the antenna characteristics in the algorithms. In the time-reversal based imaging algorithms [2], the antennas are most often characterized by their impulse response and otherwise assumed to have a somewhat uniform radiation pattern [6, 7]. In the frequency-domain based techniques, some attempts have been made to include the antenna characteristics in the imaging algorithms, especially in the realm of ground penetrating radar [8]. When used for breast cancer screening, the antennas are widely assumed to be point sources [4, 9].

In this paper, a method for including the complete antenna model is presented, thereby allowing for the imaging algorithm to adopt the antennas most suitable for the setup of the imaging system. The method is based on a transmission-matrix representation of the antennas in the microwave imaging system using the spherical-wave formulation. The spherical-wave formulation has been chosen due to the geometry of the imaging system under consideration in this paper. The concept is tested on a linear inverse scattering problem but is believed to be efficient when applied to Newton-based iterative nonlinear inversion schemes, similar to those described in [9, 10], as well.

This paper is organized as follows: In Section 2, the imaging system currently being developed at the Technical University of Denmark is introduced while the spherical wave expansion is incorporated into a linear-inversion algorithm based on the first-order Born approximation in Section 3. The algorithm is tested on simulated data in Section 4 and the results are compared to those obtained using a simple inversion algorithm in which the antennas are assumed to be ideal dipoles.

The time-dependency $\mathrm{e}^{-i\omega t}$ is assumed and suppressed in the frequency domain formulations throughout this paper.

2. IMAGING SYSTEM

The imaging system considered in this paper is the first-generation Physical-Anomaly Tomography (PAT) scanner developed at the Technical University of Denmark. The system is depicted in Figure 1, and consists of 32 air-supported patch antennas, designed for operating in the frequency domain at 5 GHz, positioned on the inside of a metallic hemisphere. The

Proc. 'EuCAP 2006', Nice, France
6–10 November 2006 (ESA SP-626, October 2006)

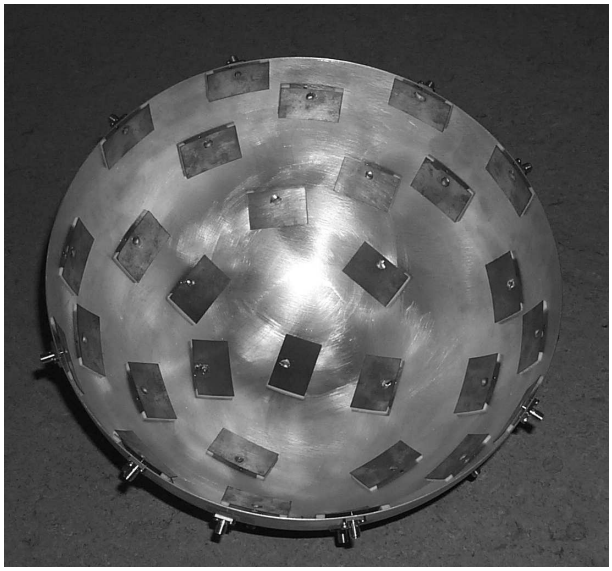

Figure 1. Picture of the PAT scanner. The system is designed to work at the frequency 5 GHz and consists of a aluminum hemisphere inside of which is positioned conformal patch antennas made of copper plating.

positions of the antennas have been determined by the use of a genetic algorithm to provide the best possible spacial coverage on the hemisphere.

The metallic hemisphere has a radius of 15 cm and the square patch antennas have been shaped to be conformal with the hemispherical ground plane. Each of the air-supported antennas are identical with the dimensions 26.9 mm by 40 mm and a schematic of an antenna is seen in Figure 2. The distance between the patches and the hemisphere is $h = 2$ mm and the feed is positioned $l_f = 7$ mm from the edge of the patch.

The antennas are predominantly linearly polarized although the axial ratio of the polarization ellipse is not well-defined inside the imaging domain due to the presence of the metallic hemisphere.

Each antenna is connected to a network analyzer through a coaxial cable and a switching network. It is assumed that the only propagating wave modes in the coaxial cables are a TEM wave propagating towards the antenna and a TEM wave propagating away from the antenna. The wave propagating toward the antenna is characterized by the complex voltage v^+ and the wave propagating away from the antenna is characterized by the complex voltage v^-.

During measurements, the object to be imaged is positioned inside the metallic hemisphere and the antennas in turn acts as the transmitter. The S parameters, that is, the ratio between v^+ on the transmitting antenna and v^- on the transmitting and the 31

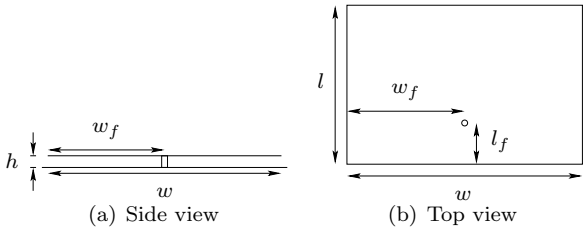

(a) Side view (b) Top view

Figure 2. Schematic of patch antenna used in the PAT scanner. Each antenna has a width of $w = 40$ mm, a length of $l = 26.9$ mm, and is positioned at a height of $h = 2$ mm above the metallic hemisphere. The feed is positioned at $w_f = 20$ mm and $l_f = 7$ mm.

receiving antennas, are then measured, providing 32 sets of 32 S parameters, one set for each antenna.

3. IMAGING ALGORITHM

To test the effect of including the antenna characteristics in the imaging algorithm, a simple linear imaging problem is investigated. By assuming that there is only a single small and low contrast object present in the imaging system, the first-order Born approximation can be used as the basis for the imaging algorithm. Under the first-order Born approximation, the scattered field $\boldsymbol{E_s}$ is assumed to be a linear function of the incident field $\boldsymbol{E_{inc}}$ given by the integral equation [11, (8.9.14)]

$$\boldsymbol{E_s}(\boldsymbol{r},\omega) = i\omega\mu \int_V \bar{\bar{\boldsymbol{G}}}(\boldsymbol{r},\boldsymbol{r'},\omega) \cdot \boldsymbol{E_{inc}}(\boldsymbol{r'},\omega) o(\boldsymbol{r'},\omega)\, \mathrm{d}^3\boldsymbol{r'}. \quad (1)$$

In this expression, $\bar{\bar{\boldsymbol{G}}}$ is the dyadic Green's function for observation point $\boldsymbol{r}$ and source point $\boldsymbol{r'}$ [11, (7.1.27)] and o is the object function given by the contrast in permittivity and conductivity of the scattering object as

$$o(\boldsymbol{r'},\omega) = \Delta\sigma(\boldsymbol{r'}) - i\omega\Delta\epsilon(\boldsymbol{r'}) = [\sigma(\boldsymbol{r'}) - \sigma_0] - i\omega\,[\epsilon(\boldsymbol{r'}) - \epsilon_0] \quad (2)$$

where ϵ_0 and σ_0 are the constitutive parameters of the background medium. It is well-known that the scattered field can be expressed in terms of the equivalent scattering current $\boldsymbol{J_{scat}}$ given by

$$\boldsymbol{J_{scat}}(\boldsymbol{r},\omega) = \boldsymbol{E_{inc}}(\boldsymbol{r},\omega) o(\boldsymbol{r},\omega). \quad (3)$$

3.1. Transmission-Matrix Representation

The antennas are characterized using a transmission-matrix representation based on the spherical-wave

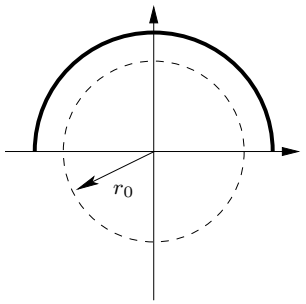

Figure 3. Schematic of the imaging domain with radius r_0 in the PAT scanner. The field inside the domain can be fully described using the $\boldsymbol{F}^{(\mathbf{1})}$ functions.

expansion. The spherical-wave expansion has been chosen due to the geometry of the PAT scanner. The spherical-wave expansion is given in terms of the power-normalized generating functions introduced in [12]. Inside the imaging domain of the PAT scanner, shown in Figure 3 with a radius of $r_0 = 12$ cm, the field can be expressed using the generating function $\boldsymbol{F}^{(\mathbf{1})}$, representing a standing wave, as

$$\boldsymbol{E}(r,\theta,\phi,\omega) = \frac{k}{\sqrt{\frac{\epsilon}{\mu}}} \cdot \sum_{s=1}^{2}\sum_{n=1}^{N}\sum_{m=-n}^{n} a_{s,m,n}\boldsymbol{F}^{(\mathbf{1})}_{\boldsymbol{s,m,n}}(r,\theta,\phi) \quad (4)$$

where $a_{s,m,n}$ is the spherical-wave expansion coefficients. The summation in n has been truncated at N. The value of N can be found using [12, (2.31)] as

$$N = \mathrm{int}(kr_0) + 10 = \mathrm{int}(104.73\ \mathrm{m}^{-1} \cdot 0.12\ \mathrm{m}) + 10 = 22. \quad (5)$$

Here it has been assumed that the radius of the imaging domain may be set to 12 cm, allowing for half a wave length of free space along the metallic hemisphere.

The transmission matrix $\underline{t}$ can now be introduced for characterizing the antennas in the PAT scanner. The transmission matrix is a column matrix satisfying the relation

$$\begin{bmatrix}\Gamma \\ \underline{t}\end{bmatrix} v^+ = \begin{bmatrix}v^- \\ \underline{a}\end{bmatrix}. \quad (6)$$

In this expression, Γ is the complex reflection coefficient measured at the terminal of the antenna, $\underline{a}$ is a column matrix holding the spherical-wave coefficients, and v^+ and v^- is the voltages of the wave incident on and reflected back into the terminals of the antenna as described in Section 2. The transmission matrix for each of the antennas in the PAT scanner can be found by using the orthogonality of the spherical-wave functions as described in [12, Sec. A.1.4].

3.2. Receiving Characteristics from Transmission Matrix

To obtain a relation between the equivalent scattering current and the change in the measured S parameters, the theorem of reciprocity [13, Eq.(1.67)] has been applied. The approach taken is similar to that used in [12, Sec. 2.3.2], and the resulting expression for the voltage v^-, characterizing the wave propagating away from any one of the antennas operating in receiver mode is given by

$$v^- = \frac{-Z_{\mathrm{coax}}k}{2\sqrt{\frac{\epsilon}{\mu}}} \int_V \boldsymbol{J}_{\mathrm{scat}}(\boldsymbol{r'}) \cdot \sum_{s=1}^{2}\sum_{n=1}^{N}\sum_{m=-n}^{n} \Big[t_{s,m,n}\boldsymbol{F}^{(\mathbf{1})}_{\boldsymbol{s,m,n}}(\boldsymbol{r'})\Big]\, \mathrm{d}^3\boldsymbol{r'} \quad (7)$$

with Z_{coax} being the characteristic impedance of the coaxial cable. By using the expression for the equivalent scattering current given in (3), the following expression is found for the change in the measured S parameters as a function of the object function

$$S_{r,t} = \frac{v_r}{v_t} = \frac{-Z_{\mathrm{coax}}k^2}{2\frac{\epsilon}{\mu}} \int_V o(\boldsymbol{r'}) \cdot \sum_{s_t=1}^{2}\sum_{n_t=1}^{N}\sum_{m_t=-n_t}^{n_t} \Big[t^{(t)}_{s_t,m_t,n_t}\boldsymbol{F}^{(\mathbf{1})}_{\boldsymbol{s_t,m_t,n_t}}(\boldsymbol{r'})\Big] \cdot \sum_{s_r=1}^{2}\sum_{n_r=1}^{N}\sum_{m_r=-n_r}^{n} \Big[t^{(r)}_{s_r,m_r,n_r}\boldsymbol{F}^{(\mathbf{1})}_{\boldsymbol{s_r,m_r,n_r}}(\boldsymbol{r'})\Big] \mathrm{d}^3\boldsymbol{r'}, \quad (8)$$

where the transmission coefficients of the transmitting and receiving antennas are given by $t^{(t)}$ and $t^{(r)}$, respectively. The forward model of the imaging problem can now be constructed by the 32^2 integral equations obtained when using all possible combinations of transmitting and receiving antennas. Due to the reciprocity of the problem, one half of the equations are identical to the other half and may be omitted. It has, however, been found that the impact of noise decreases if all of the equations are utilized in the forward model.

3.3. Matrix Equation

The imaging algorithm can now be constructed by casting the integral equations for the scattering parameters into a discrete matrix equation. The transformation from integral equation to matrix equation is accomplished by dividing the imaging domain inside the PAT scanner into N_v voxels, each characterized by the position of their center $\boldsymbol{r_n}$ and their volume v_n. The voxels are assumed to be so small that both the object function o and the spherical vector

functions $\boldsymbol{F^{(1)}}$ may be considered constant within the individual voxels.

The discretization leads to the following matrix equation

$$\underline{\underline{P}}\,\underline{o} = \underline{s}. \tag{9}$$

In this expression, the matrix

$$\underline{\underline{P}} = \begin{bmatrix} P(1,1,\boldsymbol{r_1}) & \dots & P(1,1,\boldsymbol{r_{N_v}}) \\ P(1,2,\boldsymbol{r_1}) & \dots & P(1,2,\boldsymbol{r_{N_v}}) \\ \dots & \dots & \dots \\ P(32,32,\boldsymbol{r_1}) & \dots & P(32,32,\boldsymbol{r_{N_v}}) \end{bmatrix} \tag{10}$$

holds the discrete form of the forward model from the transmitting antenna to the receiving antenna. When using the PAT scanner, the matrix has 1024 rows, which is the number of S parameters available. The complex function P is given by

$$P(r,t,\boldsymbol{r_n}) = \frac{-Z_{\text{coax}}k^2}{2\frac{\epsilon}{\mu}} v_n \sum_{s_t=1}^{2}\sum_{s_r=1}^{2}\sum_{n_t=1}^{N}\sum_{n_r=1}^{N}\sum_{m_t=-n_t}^{n_t}\sum_{m_r=-n_r}^{n_r} \left[t^t_{s_t,m_t,n_t} \cdot t^r_{s_r,m_r,n_r} \boldsymbol{F^{(1)}_{s_t,m_t,n_t}}(\boldsymbol{r_n}) \cdot \boldsymbol{F^{(1)}_{s_r,m_r,n_r}}(\boldsymbol{r_n})\right] \tag{11}$$

wherein it has been applied that the spherical-vector functions are considered constant in each of the small voxels. When filling the matrix $\underline{\underline{P}}$ the most time consuming operation by far is the calculation of the spherical-wave functions. These, however, need only to be calculated once for each voxel and can then be reused for all of the antenna combinations.

The column matrix $\underline{o}$ in (9) holds the unknown object function for each of the N_v voxels in the imaging domain. When operating in a free-space setup, the imaging domain is typically divided into box-shaped voxels with side lengths of $\frac{\lambda}{10}$. At 5 GHz this implies a side length of 6 mm and using a hemispherical imaging domain with a radius of 12 cm the total number of voxels is $N_v = 14943$. This will also be the number of columns in the matrix $\underline{\underline{P}}$.

The column-matrix on the right-hand side of (9)

$$\underline{s} = \begin{bmatrix} S^{obj}_{1,1} - S^{cal}_{1,1} \\ S^{obj}_{1,2} - S^{cal}_{1,2} \\ \vdots \\ S^{obj}_{32,32} - S^{cal}_{32,32} \end{bmatrix} \tag{12}$$

holds the difference in the S parameters measured with the object inside the PAT scanner and the S parameters measured when no object is present. The subtraction of the calibration measurement is necessary because the matrix $\underline{\underline{P}}$ does not include information on the background field in the PAT scanner.

The matrix equation can be solved using the truncated singular value decomposition method [14, Sec. 3.2] or similar methods such as the iterative conjugated gradient line search algorithm [14, 6.3].

3.4. Dipoles in Free Space

For comparison a simple algorithm using the assumption that the antennas in the PAT scanner are adequately represented using dipoles has been derived. The antennas are assumed to be dipoles positioned in free space and the voltage measured on the terminals of the antennas is assumed to be equal to the component of the scattered field parallel to the dipole.

Using (1), the voltage across the terminals of the $\hat{\boldsymbol{p}}_{\boldsymbol{r}}$-directed receiving antenna is given as

$$v_r = i\omega\mu \int_V \hat{\boldsymbol{p}}_{\boldsymbol{r}} \big(\bar{\bar{\boldsymbol{G}}}(\boldsymbol{r_r},\boldsymbol{r'},\omega) \cdot \boldsymbol{E_{inc}}(\boldsymbol{r'},\omega) o(\boldsymbol{r'},\omega)\big)\,\mathrm{d}^3\boldsymbol{r'}. \tag{13}$$

The incident field $\boldsymbol{E_{inc}}$ at the point $\boldsymbol{r'}$ is found using the Green's function and the dipole moment of the $\hat{\boldsymbol{p}}_{\boldsymbol{t}}$ directed transmitting antenna [15, (10)] as

$$\boldsymbol{E_{inc}}(\boldsymbol{r'},\omega) = i\omega\mu I(\omega)\bar{\bar{\boldsymbol{G}}}(\boldsymbol{r'},\boldsymbol{r_t},\omega)\cdot\hat{\boldsymbol{p}}_{\boldsymbol{t}} = i\omega\mu\frac{v_t}{Z_{\text{in}}}\hat{\boldsymbol{p}}_{\boldsymbol{t}}\cdot\bar{\bar{\boldsymbol{G}}}(\boldsymbol{r'},\boldsymbol{r_t},\omega) \tag{14}$$

with Z_{in} being the impedance at the terminals of the antennas.

By use of this expression, the expression for the S parameters can be found as

$$S_{r,t} = \frac{v_r}{v_t} = \frac{-\omega^2\mu^2}{Z_{\text{in}}} \int_V \left[\hat{\boldsymbol{p}}_{\boldsymbol{r}}\cdot\bar{\bar{\boldsymbol{G}}}(\boldsymbol{r_r},\boldsymbol{r'},\omega)\right] \cdot \left[\hat{\boldsymbol{p}}_{\boldsymbol{r}}\cdot\bar{\bar{\boldsymbol{G}}}(\boldsymbol{r_r},\boldsymbol{r'},\omega)\right] o(\boldsymbol{r'},\omega)\,\mathrm{d}^3\boldsymbol{r'}. \tag{15}$$

This expression can be cast into a matrix equation in much the same way as the expression for the algorithm including the antenna characteristics. The resulting expression is

$$\underline{\underline{P}}_{fs}\,\underline{o} = \underline{s} \tag{16}$$

where the elements of the matrix $\underline{\underline{P}}_{fs}$ are given by

$$P_{fs}(r,t,\boldsymbol{r_n}) = \frac{-\omega^2\mu^2 v_n}{Z_{\text{in}}} \left[\hat{\boldsymbol{p}}_{\boldsymbol{r}}\cdot\bar{\bar{\boldsymbol{G}}}(\boldsymbol{r_r},\boldsymbol{r_n},\omega)\right] \cdot \left[\hat{\boldsymbol{p}}_{\boldsymbol{r}}\cdot\bar{\bar{\boldsymbol{G}}}(\boldsymbol{r_r},\boldsymbol{r_n},\omega)\right]. \tag{17}$$

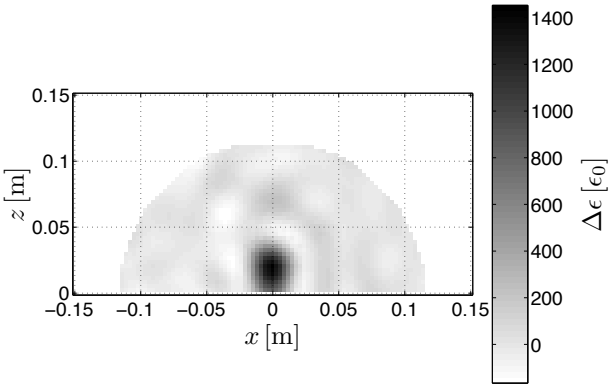

(a) Ideal dipoles in free space

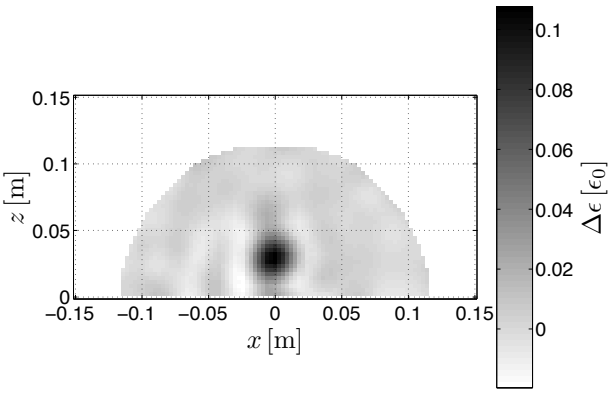

(b) Antenna models included

Figure 4. Results obtained using (a) the algorithm assuming ideal dipoles and (b) the algorithm including the antenna models for constant $y = 0$. The spherical scatterer is centered at $(x, y, z) = (0, 0, 3\ cm)$, has a radius of 1.5 cm, and a contrast of $\Delta\epsilon = 0.1\epsilon_0$.

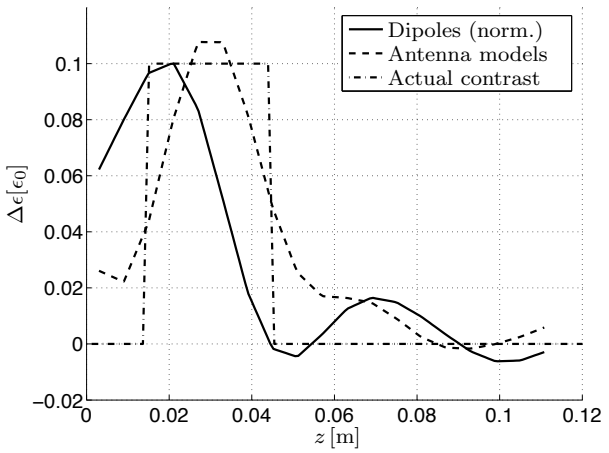

Figure 5. Comparison of contrast obtained using the two different algorithms along the line from $(x, y, z) = (0, 0, 0)$ to $(x, y, z) = (0, 0, 15\ cm)$. The result of the inversion with the algorithm using the dipole assumption has been normalized to allow for a comparison of its ability to detect the location of the scatterer.

4. TEST OF ALGORITHM

The algorithm has been tested using simulated data. In the simulation, the PAT scanner is operating in a free-space setup with the only other object present being the scattering object inside the system. The complete setup is simulated using a method of moments code [16].

In the simulation, a single spherical object is positioned inside the PAT scanner. The radius of the object is 1.5 cm and the center of the object is positioned at $(x_c, y_c, z_c) = (0, 0, 3\ \text{cm})$. The scatterer has a relative permittivity of $\epsilon_r = 1.1$, implying $\Delta\epsilon = 0.1\epsilon_0$.

The results of the inversion using the algorithm including the antenna characteristics and the algorithm assuming dipoles positioned in free space are seen in Figure 4. Both algorithms seem to detect the position of the scatterer. The algorithm including the antenna models, however, is also capable of recreating the actual contrast whereas the algorithm using the simple dipole models yields a contrast which is far from the actual contrast of the scatterer. Also, the position of the scatterer is slightly offset in the negative $\hat{\boldsymbol{z}}$ direction in the image created by the algorithm based on the dipole assumption whereas the inclusion of the full antenna models allows for a very accurate estimate of the position and extend of the scatterer.

In Figure 5, the contrast obtained using the two different algorithms along the line $(x, y) = (0, 0)$ are plotted against the actual contrast. The contrast obtained with the ideal-dipole algorithm has been normalized, allowing for a better comparison. In this plot it is clearly seen that the algorithm including the antenna models detects the position of the scatterer very accurate with the maximum contrast being at the center of the scatterer, and returns an accurate estimate of the contrast of the scatterer. The offset in the negative $\hat{\boldsymbol{z}}$ direction of the simple dipole-based model is also clearly seen.

Similar results have been observed as the scatterer is moved around inside the PAT scanner; the inclusion of the full antenna models in the algorithm yields results that are clearly better than when the dipole model is used, both in terms of location of the object and in terms of the level of the contrast.

5. CONCLUSION

The concept of including the antenna characteristics in frequency-domain microwave imaging has been shown to improve the image quality when applied

to a linear imaging algorithm. The algorithm was tested on a simulated model of the first-generation PAT scanner developed at the Technical University of Denmark, and compared to an algorithm in which the antennas were assumed to be ideal dipoles, the performance of the new algorithm was superior in terms of determining both location and contrast of the scattering object. The antenna characteristics were defined in terms of the spherical-wave expansion to fit the geometry of the measurement system.

The incorporation of the antenna-characteristics in an iterative Newton-based non-linear is the subject of ongoing research and is believed to be achievable with relative ease. Furthermore, the scattering-matrix representation of the antennas in the imaging system can easily be reformulated in terms of cylindrical or plane waves if the algorithm is to be applied for an imaging system with a different geometrical setup of the antennas.

ACKNOWLEDGMENTS

The Danish Technical Research Council is acknowledged for supporting the work of Tonny Rubæk and Peter Meincke. Mario Fernandez is acknowledged for creating the genetic algorithm for determining the position of the antennas.

REFERENCES

1. E. Fear, P. Meaney, and M. Stuchly, "Microwaves for breast cancer detection?" *IEEE Potentials*, vol. 22, no. 1, pp. 12–18, 2003.

2. X. Li, E. Bond, B. Van Veen, and S. Hagness, "An overview of ultra-wideband microwave imaging via space-time beamforming for early-stage breast-cancer detection," *Antennas and Propagation Magazine, IEEE*, vol. 47, no. 1, pp. 19–34, 2005.

3. R. Nilavalan, J. Leendertz, I. Craddock, A. Preece, and R. Benjamin, "Numerical analysis of microwave detection of breast tumours using synthetic focussing techniques," *Antennas and Propagation Society Symposium, 2004. IEEE*, pp. 2440–2443 Vol.3, 2004.

4. P. Meaney, K. Paulsen, A. Hartov, and R. Crane, "An active microwave imaging system for reconstruction of 2-d electrical property distributions," *Biomedical Engineering, IEEE Transactions on*, vol. 42, no. 10, pp. 1017–1026, 1995.

5. P. Hashemzadeh, A. Fhager, and M. Persson, "Experimental investigation of an optimization approach to microwave tomography," *Electromagnetic Biology and Medicine*, vol. 25, no. 1, pp. 1–12, 2006.

6. E. Fear, A. Low, J. Sill, and M. A. Stuchly, "Microwave system for breast tumor detection: Experimental concept evaluation," *IEEE Antennas and Propagation Society, AP-S International Symposium (Digest)*, vol. 1, pp. 819–822, 2002.

7. C. Shannon, E. Fear, and M. Okoniewski, "Dielectric-filled slotline bowtie antenna for breast cancer detection," *Electronics Letters*, vol. 41, no. 7, pp. 11–12, 2005.

8. P. Meincke and T. Hansen, "Plane-wave characterization of antennas close to a planar interface," *Geoscience and Remote Sensing, IEEE Transactions on*, vol. 42, no. 6, pp. 1222–1232, 2004.

9. P. Meaney, K. Paulsen, and J. Chang, "Near-field microwave imaging of biologically-based materials using a monopole transceiver system," *Microwave Theory and Techniques, IEEE Transactions on*, vol. 46, no. 1, pp. 31–45, 1998.

10. D. Li, P. Meaney, and K. Paulsen, "Conformal imaging with a non-contacting microwave antenna array," *Microwave Symposium Digest, 2001 IEEE MTT-S International*, vol. 1, pp. 563–566 vol.1, 2001.

11. W. C. Chew, *Waves and Fields in Inhomogeneous Media*, ser. IEEE Press Series on Electromagnetic Waves, D. G. Dudley, Ed. New York: IEEE Press, 1995.

12. J. Hald, J. E. Hansen, F. Jensen, and F. H. Larsen, *Spherical Near-Field Antenna Measurements*, ser. IEE Electromagnetic Waves Series, J. E. Hansen, Ed. Peter Peregrinus Ltd., 1988, vol. 26.

13. R. E. Collin and F. J. Zucker, *Antenna Theory, part I.* New York: McGraw-Hill, 1969.

14. P. C. Hansen, *Rank-Deficient and Discrete Ill-Posed Problems: Numerical Aspects of Linear Inversion*, ser. Monographs on Mathematical Modeling and Computation. SIAM, 1998.

15. P. Meincke, "Linear gpr inversion for lossy soil and a planar air-soil interface," *Geoscience and Remote Sensing, IEEE Transactions on*, vol. 39, no. 12, pp. 2713–2721, 2001.

16. E. Jørgensen, J. L. Volakis, P. Meincke, and O. Breinbjerg, "Higher order hierarchical legendre basis functions for electromagnetic modeling," *IEEE Transactions on Antennas and Propagation*, vol. 52, no. 11, pp. 2985–2995, nov 2004.